Piezo - Photocatalytic Performance of Fe- Doped $BaTiO_3$ Compounds

Wycliffe M. Isoe[1,5]*, Bernard Omogo[1], Onesmus M. Munyati[2], Christopher M. Maghanga[4,5], Sylvester Hatwaambo[2], Maurice M. Mwamburi[3,5], Nicholas O. Ongwen[1,5], David Machiri[1], Benjamin V. Odari[1,5], Maxwell J. Mageto[1,5]

[1] *Department of Physics, Masinde Muliro University of Science and Technology, P.O. Box 190 Kakamega, Kenya*

[2]*Department of Physics, School of Natural Sciences, University of Zambia, P. O. Box 32379, Lusaka, 10101 Zambia*

[3]*Department of Physics, University of Eldoret, P.O. Box 1125 Eldoret, Kenya.*

[4]*Department of Physical & Biological Sciences, P.O. Box Private Bag Kabarak, Nakuru, Kenya*

[5] *Materials Research Society of Kenya, P.O. Box 15653-00503 Nairobi, Kenya*

Abstract

Barium titanate ($BaTiO_3$) is a feasible photocatalytic semiconductor. This has been demonstrated in both experimental and computational studies on the material. To enhance its photocatalytic performance under visible light, this study investigated the effect of introducing iron (Fe) dopant into its structure. The undoped and Fe-doped $BaTiO_3$ films were synthesized and deposited on glass substrate using the spin coating technique and its photocatalytic activity was evaluated through photodegradation of methyl blue aqueous solution. The bandgap of the synthesized $BaTiO_3$ reduced from 3.26 eV to 1.59 eV for the undoped and the 0.5%wt Fe doped samples, respectively. Further analysis revealed that 0.5%wt Fe had the best photocatalytic performance with a photo-degradation constant of $2.37 \times 10^{-3}\, m^{-1}$. The effect of Fe doping on the structural and electronic properties of $BaTiO_3$ was further investigated by employing the Density Functional Theory. The electronic structures showed that Fe creates some defect states in the energy band, which forms weak coordinate covalent bond that greatly reduces the bandgaps of the doped materials. These results demonstrate the potential of employing Fe-doped $BaTiO_3$ as a visible light photocatalytic material.

Introduction

Tenacious organic compounds in industrial wastewater and their proper removal have emerged as a crucial problem to waste water treatment plants. Among many proposed methods, photocatalysis stands out as an efficient and sustainable oxidation technology in waste water treatment, since it allows complete mineralization of toxins (Dooyoung, Vinh, & Thomas, 2024). Further, the development of visible light photocatalysts to address water pollution is essential since visible light constitutes a good fraction of the solar spectrum (Jiaguo, Liuyang, Linxi, & Bicheng, 2023). Research has suggested many photocatalysts, the semiconductor barium titanate

($BaTiO_3$), being among them. $BaTiO_3$ stands out to be a promising photocatalytic compound, owing its inherent chemical activity (Gopal & Mira, 2022).

Semiconductor – based photocatalysts have drawn high interest in the recent past, majorly due their ability to reduce organic pollutants into less harmful and environmentally friendly compounds at low costs (Huaitao, Beibei, Wei, & Junjiao, 2022). Among many existing photocatalytic materials; titanium oxide and zinc oxide are largely being investigated due to their chemical stability, high photocatalytic activity, and non-toxicity (Chukwuka, Ilknur, & Vassilis, 2022). However, these and many other photocatalysts have some shortcomings: Firstly, their large bandgap (~3.2eV) makes them active under ultra-violet (UV) radiation, which accounts for about 4% of total solar radiation (Jinkai, Masato, Ajay, & Masakazu, 2007). Moreover, water treatment by UV radiation, in most cases, leads to high energy consumption and bacteria regrowth after the process (Maria, et al., 2021). Secondly, many photocatalysts do not have the requisite optical properties to start the process of microbial inactivation, and thirdly, they are not magnetic, hence do not promote recyclability and recovery by magnetic force (González-Fernández, Gómez-Pastora, Bringas, Zborowski, & Chalmers, 2021).The metal ions in magnetic photocatalytic materials would accelerate the charge transfer and as a result reduce the recombination rate which subsequently promotes photocatalytic activity (Surassa, Hataikarn, Khatcharin, Phanichphant, & Natda, 2014).

The perovskite barium titanate ($BaTiO_3$) compound has been studied both experimentally and theoretically for applications as oxide photocatalyst, and has shown promising results (Lee, et al., 2013; Liu & Sun, 2012; Cui, Briscoe, & Dunn, 2013; Kappadan, Gebreab, Thomas, & Kalarikkal, 2016). To further enhance its photocatalytic activity under visible light, this study investigated the effect of introducing Iron (Fe) dopant on its bandgap as well on its photocatalytic performance of $BaTiO_3$.

2 Materials and Methodology

2.1 Synthesis of Undoped and Fe-doped $BaTiO_3$ Samples

Undoped and Fe-doped $BaTiO_3$ films were synthesized through a sol-gel synthesis technique. The initial materials that were employed were barium acetate ($Ba(C_2H_3O_2)_2$), titanium (iv) isopropoxide [$Ti(C_{12}O_4H_{28})$], and ferric chloride ($FeCl_2.6H_2O$). The initial materials were weighed according to the stoichiometric quantities and mixed thoroughly in aqueous phases for the homogenization of the compositions. Firstly, the measured amounts of ferric chloride and barium acetate were mixed in heated glacial acetic acid. The resulting solution was stirred constantly until all the particles were dissolved. Secondly, the suitable amount of titanium (iv) isopropoxide was dissolved in 2-methoxyethonal and was added to the already prepared solution under continuous stirring. The stabilizer ethylene glycol was added to this solution in the ratio 1:3 proportion to the glacial acetic acid. Finally, the precursor solutions of $BaTi_{1-x}O_3Fe_x$ with concentrations x = 0.0, 0.05, 0.1, 0.2, 0.3 and 0.4 were obtained. The molarity of all solutions prepared was maintained at 0.4 M for spin coating on microscope glasses. Before spin coating at 3000 rev./min for 45 seconds, the microscope glass substrates were cleaned with acetone, isopropyl alcohol and deionized water at 80 ℃ for 10 minutes in each and then dried in air. A thin film comprised of three layers of coating and each layer was subjected to a controlled heat treatment cycle in a rapid thermal processor. Every spin coated layer was dried at 100 ℃ for 10

minutes in a muffle furnace. The coated samples were then annealed at different temperatures; 400℃, 500℃, and 600℃ for two hours for each sample. Table 1 shows the specific amounts of compounds employed for the synthesis of $BaTi_{1-x}O_3Fe_x$ samples.

2.2 Density Functional Theory Study on Undoped and Fe-doped $BaTiO_3$ samples

The theoretical calculations of undoped and Fe – doped $BaTiO_3$ were performed by employing Quantum Espresso (QE) package, which is based on the density functional theory (DFT), employing the plane wave pseudopotential (PWP) formalism. The local density approximation (LDA) with an ultra-soft pseudopotential was employed. Vanderbilt ultra-soft pseudopotentials were adopted for each type of ion, in which 5s, 5p and 6s electrons for Ba; the 3s, 3p, 3d and 4s electrons of Ti; the 2s and 2p electrons of O; and the 3s, 3p, 4s and 4p electrons of Fe were all treated as valence states.

The 3d tetragonal structure that was investigated belongs to space group P4mm. The crystallographic information files of $BaTiO_3$ were obtained from crystallography open database. The initial data for this simulation was generated through convergence tests on the structure that were done by self-consistent field (SCF) calculations to determine the convergence of the plane wave cut-off (ecutwfc), lattice parameters as well as the charge density cut-off (ecutrho) with the total energy. To make it possible for doping, a $2\times2\times2$ supercell was generated containing 40 atoms as shown in figure 1. The wave function was expanded to 1080 eV plane wave kinetic energy cutoff for iron doped samples. Generalized Gradient Approximation (GGA) suggested by Perdew, Burke and Ernzerhof (PBE) was employed for evaluating the exchange correlation energy.

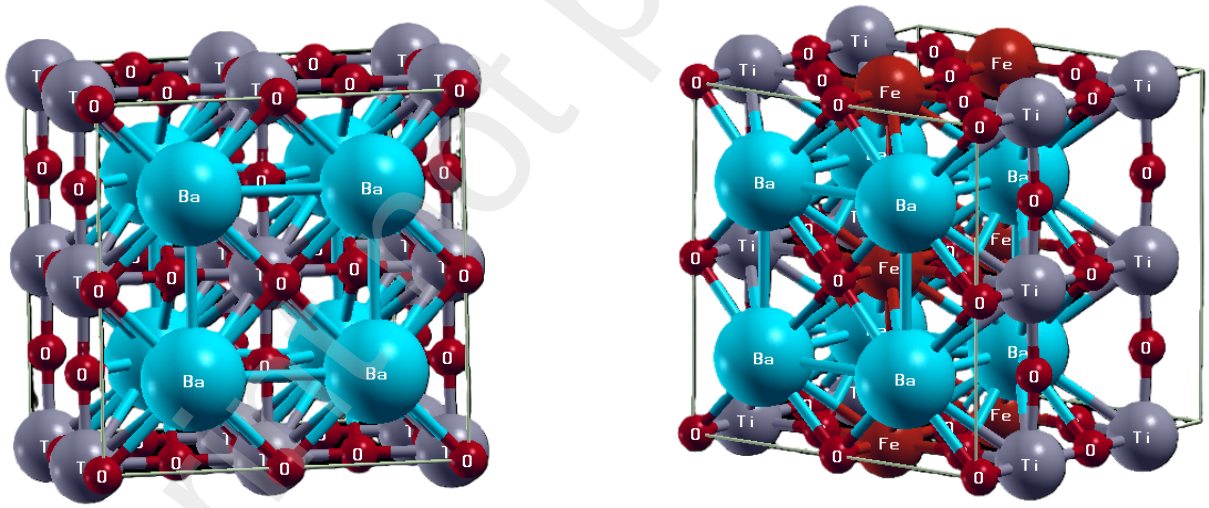

(a) (b)

Figure 1. The (2x2x2) crystal structure of (a) Undoped $BaTiO_3$ and (b) 0.5%wt Fe-doped $BaTiO_3$

Table 1: The specific amounts of compounds employed for the synthesis of $BaTi_{1-x}O3Fe_x$ samples

Material	Dopant concentrations					
	x=0.0M	x=0.05M	x=0.1M	x=0.2M	x=0.3M	x=0.4M
Barium acetate	1.53 g	1.53 g	1.53 g	1.53 g	1.53 g	1.53 g
Titanium (iv) isopropoxide	2.11ml	2.11ml	2.11ml	2.11ml	2.11ml	2.11ml
Ferric chloride	0.0 g	0.081 g	0.162 g	0.324 g	0.486 g	0.648 g
Glacial acetic acid	15 ml	15 ml	15 ml	15 ml	15 ml	15 ml
2-methoxyethanol	15ml	15 ml	15 ml	15 ml	15 ml	15 ml
Ethylene glycol	5 ml	5 ml	5 ml	5 ml	5 ml	5 ml

2.3 Optical Characterization of the Doped and Undoped Samples

The optical properties of the undoped $BaTiO_3$ and Fe–doped $BaTiO_3$ thin films were investigated using UV-VIS spectroscopy (Shimandzu UV-VIS 2600) in the wavelength range 300 to 900 nm. This range was chosen since it covers the wavelength spectrum applicable to $BaTiO_3$ wide-band gap nature and absorption edge, all of which are crucial in computing photocatalytic reactions.

Further optical properties were modelled using SCOUT software (Theiss 2002) where the obtained experimental spectra were fitted to the simulated spectra. The software is a package of a variety of models. The choice of the model to be used in fitting of the spectra depends on the material being studied and the range of the spectrum being employed. The models employed in this work were Drude, Kim, Tauc-Lorentz, the harmonic and OJL interband transition model.

2.3 Photocatalytic Examination of the Doped and Undoped Samples

In Photocatalytic degradation examination, methylene blue (MB) dye was employed as an indicative pollutant of the water. The normal degradation process begins with the MB dye adsorption, and the dye concentration reduces in the adsorption process. Once adsorption-desorption equilibrium has been achieved, the photocatalytic process begins with light illumination which leads to photogeneration of charge carriers. The photocatalytic efficiency for

pure and Fe-doped $BaTiO_3$ was evaluated under visible light. A 100W halogen lamp was employed as a source of visible light.

At 30min intervals for 4hours, 2ml of the photodegraded methylene blue solution was taken and analyzed by recording the change in the absorption peak at 664nm from the absorption spectrum in the range 400-800nm.

The pseudo-first-order kinetic model was employed to measure the photocatalytic activity of the samples by finding the kinetic rate constant, k (min^{-1}). The pseudo first-order is as shown in equation 1.

$$-\ln\left(\frac{c}{c_0}\right) = kt \qquad [1]$$

Where k is the apparent rate constant (min^{-1}), c_o is the initial concentration of MB, and c is the concentration of MB at different reaction times (t)

3. Results and Discussion

3.1 Absorbance of Undoped and Fe-Doped $BaTiO_3$ Thin Films

UV-vis spectrum is important, since it can equip us with knowledge about the energy band structure of electrons on valence band and conduction band (Tang, Prasad, Sanjines, Schmid, & Levy, 1994; Restiani & Asep, 2022). The absorption between 300-500nm increased with increase in Fe doping concentration, which is attributed to the increase in carrier concentration. From figure 2, it is observed that the absorption edge shifts towards longer wavelength with increase in Fe doping concentration. This can be attributed to the reduction in bandgap.

It's further observed that absorbance of the films increased with increase in Fe doping concentration to optimum doping concentration of 0.3%wt before it begun to drop again. Doping comprises adding low level of impurities, which increases the population of charge carriers in the material, which in turn affects the material properties (Leyland, et al., 2016).

Figure 2 also shows absorption spectra of the films annealed at 400℃, 500℃ and 600℃ for 1hour. The absorption edge of the films annealed at 600℃ is found to be higher than that of the films annealed at 400℃ and 500℃. This can be understood to mean that the films' crystallinity increases with increase in annealing temperature. It can thus, be concluded that annealing leads to improvement of optical properties of materials.

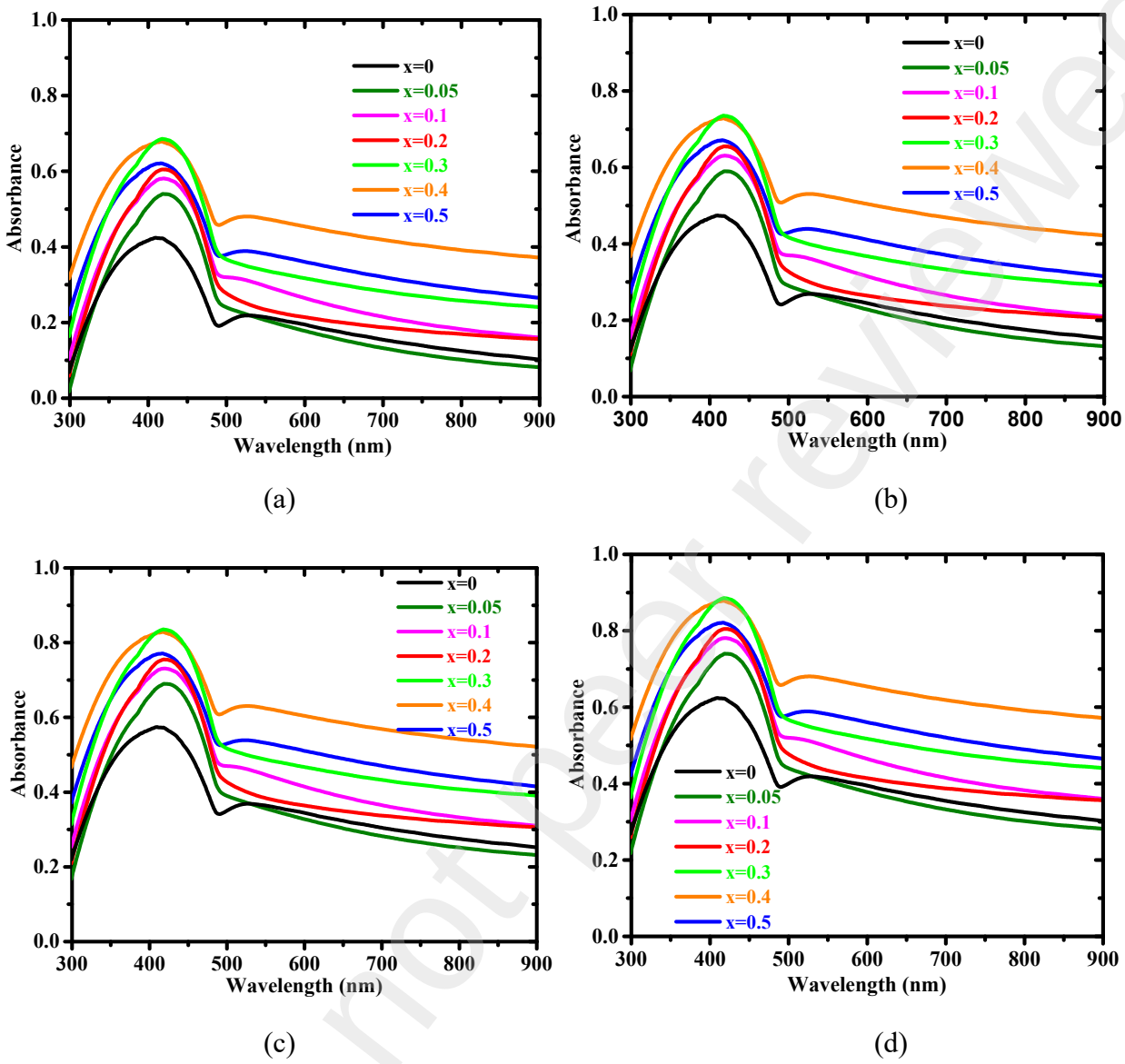

Figure 2. Absorbance Spectra of Undoped and Fe-Doped $BaTiO_3$ Compounds for (a) Unannealed samples and samples annealed at (b) 400℃, (c) 500℃ and (d) 600℃

The bandgap of the synthesized samples in figures 3 were assessed by employing the Tauc's plot (Granqvist, 1995), and the bandgap was found to reduce in the range 3.26eV-1.59eV. It was observed that there is a significant decrease in the bandgap with increase in Fe doping. This decrease in the bandgap can be described by electronic states of the highest occupied molecular orbital and the lowest unoccupied molecular orbital (Zhang, et al., 2020). The substitution of Ti^{4+} with Fe^{3+} ends in energy states above the valence band and below conduction band, which can be associated with decrease in bandgap with increase in Fe doping concentration (Sharma & Vaish, 2021). Thus, the noticeable reduced bandgap means that the material can now be employed for visible light activation photocatalytic reactions.

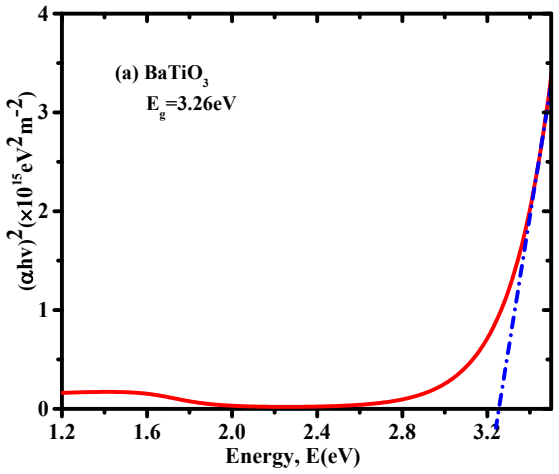

(a)

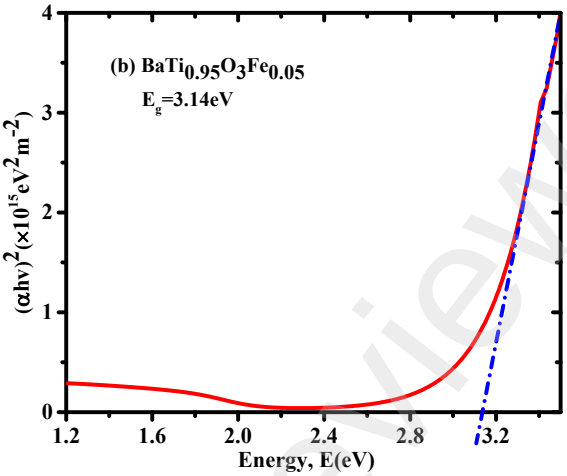

(b)

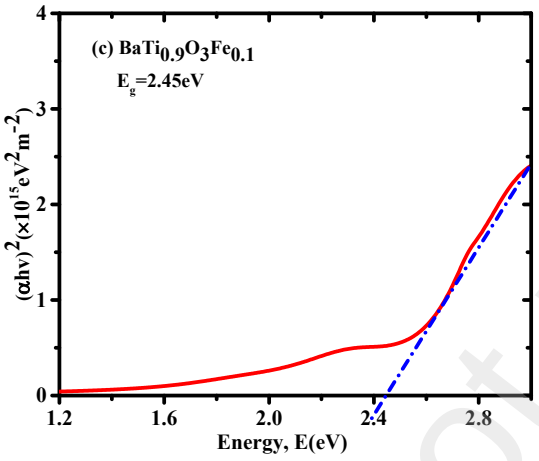

(c)

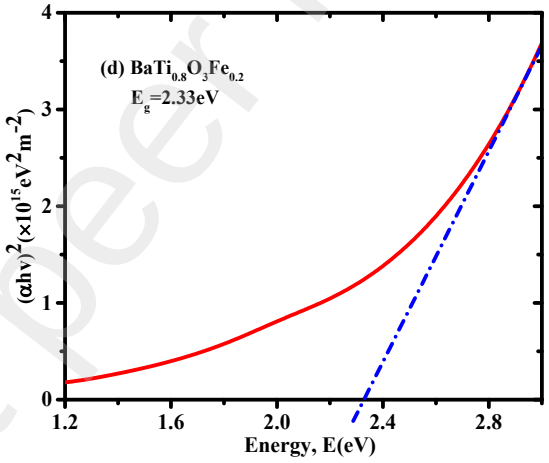

(d)

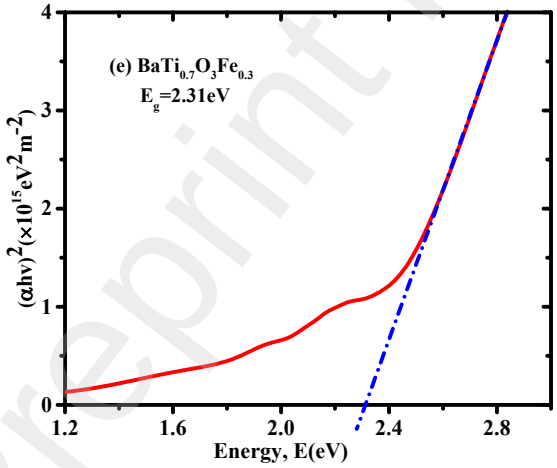

(e)

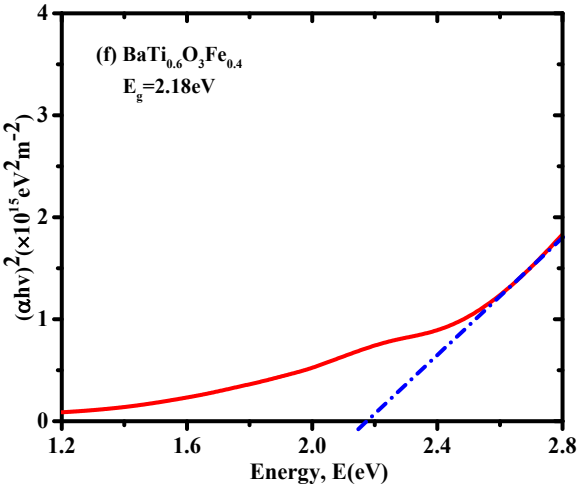

(f)

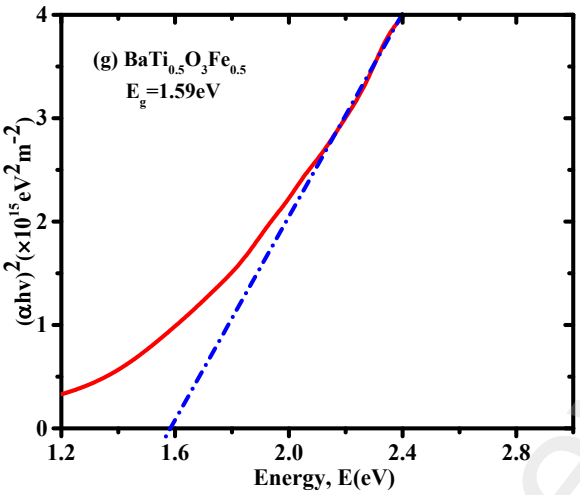

(g)

Figure 3. Energy Bandgap $BaTi_{1-x}O_3Fe_x$ Thin Films for Various Fe Concentration (a) $x = 0$ %wt, (b) 0.05%wt, (c) 0.1%wt, (d) 0.2%wt, (e) 0.3%wt ,(f) 0.4%wt and (g) 0.5%wt)

3.2 Electronic Band Structure and Density of states

In dielectric physics, the dielectric characteristics are intimately connected to the electronic structure of the material, for instance the energy band structure and the density of states (Fang, 2023). Thus, the electronic band structure and density of states (DOS) of undoped and Fe-doped $BaTiO_3$ samples were studied computationally and the results presented in figures 4-7. From figures 4, the band gap of undoped $BaTiO_3$ was found to be 1.8 eV, which is in agreement with other reported work (Aminul, Addul, & Meherun, 2017). The other bandgap values are recorded in table 2. The computed energy-band structures were done by employing Generalized Gradient Approximations (GGA) along high-symmetry directions in the Brillouin Zone (BZ). The total density of states (TDOS) and the partial density of states (PDOS) of the samples are as well presented.

From figure 4, it is observed that the top of the valence band and the bottom of the conduction lie at the *B* point and *Γ* point of Brillouin zone respectively. Thus, the undoped $BaTiO_3$ is an indirect band gap semiconductor. The band gaps, as observed in figures 5-7, greatly reduced in the Fe-doped $BaTiO_3$ systems. The reduction of bandgaps is due to the presence of the defect band. The shift in the points of Brillouin zones, as observed, is also evidence of the presence of the defect energy band. Further, it was observed that in the undoped $BaTiO_3$ band structure, the lowest conduction band is quite flat from *Γ* to *B,* which is usual for many ABO_3 perovskite ferroelectrics (Hellwege, 2016). The PDOS figures show that the valence band majorly constitutes of the Fe 3d; O 2p; Ti 3d; and Ba 5p electrons. The major contribution to the conduction band arises from Fe 3d and Ti 3d electrons. The sharp peaks observed, majorly arise from the effect of Fe dopant.

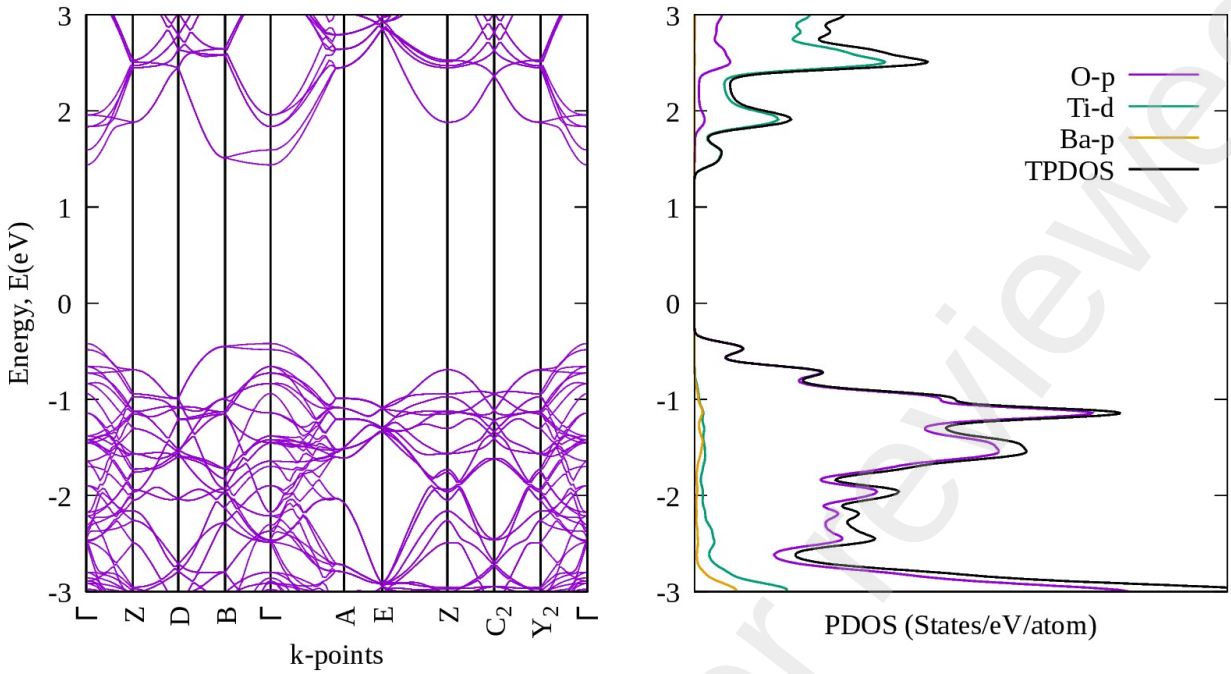

Fig. 4. (a) Electronic Band structure and (b) PDOS of Undoped $BaTiO_3$

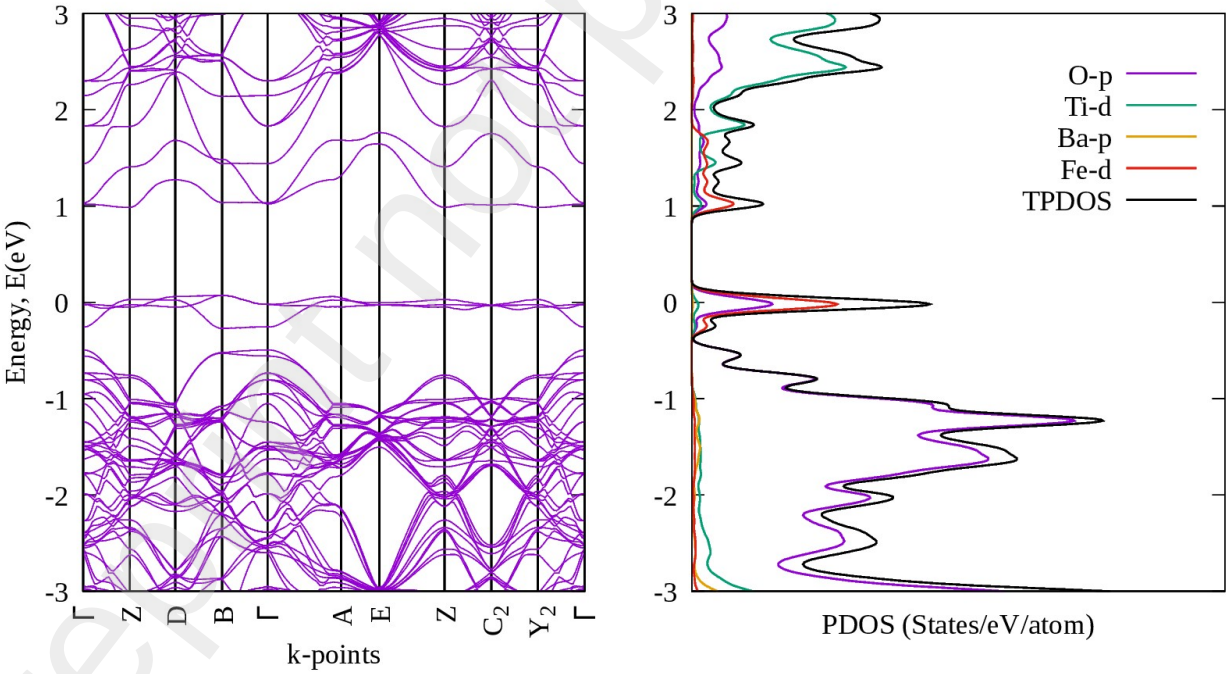

Fig. 5. (a) Electronic Band structure and (b) PDOS of 2.5% Fe- $BaTiO_3$

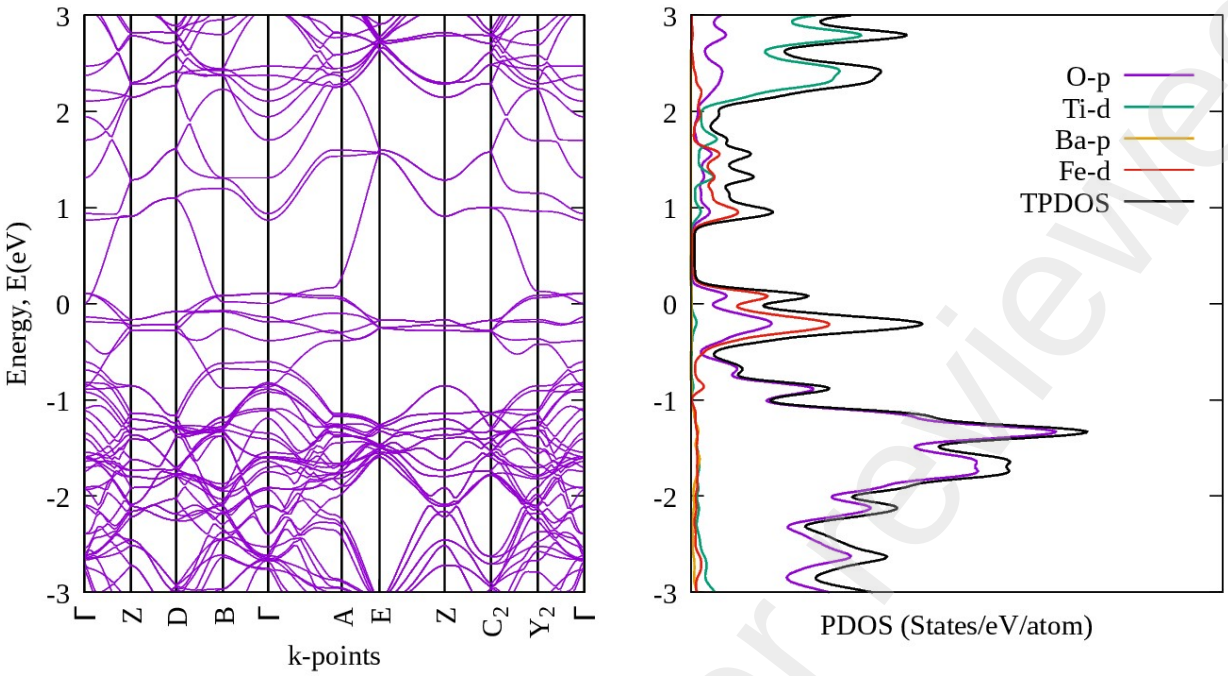

(a) **(b)**

Fig. 6. (a) Electronic Band structure and (b) PDOS of 5% Fe- $BaTiO_3$

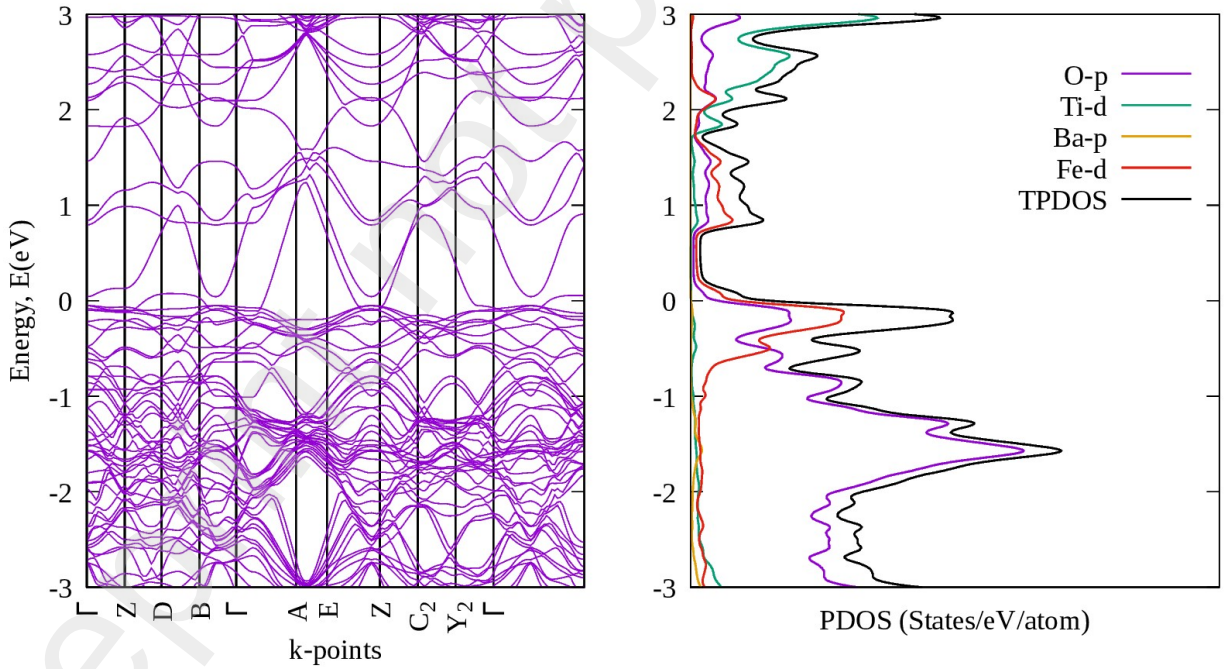

(a) (b)

Fig. 7. (a) Electronic Band structure and (b) PDOS of 7.5% Fe- $BaTiO_3$

Table 2: Band Values of undoped and Fe - doped $BaTiO_3$ Systems

System	*Brillouin zone*	*E_g (eV)*
Undoped $BaTiO_3$	*Γ - B*	1.86
2.5% Fe - doped $BaTiO_3$	*Γ - B*	0.98
5% Fe - doped $BaTiO_3$	-	Semi-metallic
7.5% Fe - doped $BaTiO_3$	-	Semi-metallic

3.3 Structural properties of undoped and Fe-doped BaTiO3 samples

In order to obtain the optimized structure of $BaTiO_3$, a number of calculations were done and to obtain relaxed structures, ionic positions and lattice geometry were optimized, resulting theoretical estimated lattice parameters shown in table 3.

Table 3: The theoretical and experimental lattice parameters of undoped and Fe- $BaTiO_3$ perovskite

	$BaTiO_3$			**Fe- doped $BaTiO_3$**	
	$a = b$ $(\mathring{A})$	$c(\mathring{A})$	$V(\mathring{A}^3)$	a($\mathring{A}$)	$V(\mathring{A}^3)$
Our DFT calculated values	7.77	8.11	489.60	7.91	495.63
Experimental Values (Nurazila, Mahmood, Thye, & Julie, 2024)	8.00	8.02	513.28	8.04	519.72
Other DFT calculated values (Aminul, Addul, & Meherun, 2017)	7.96	8.16	516.77	8.42	596.95

The calculated lattice parameters for undoped and Fe-$BaTiO_3$ were found be in good agreement with experimental values (Nurazila, Mahmood, Thye, & Julie, 2024; Hellwege, 2016) and other theoretical calculations (Aminul, Addul, & Meherun, 2017).

3.4 Photocatalytic Performance of Synthesized undoped and Fe-doped Films

Figure 8a shows the degradation efficiencies of MB solution over pure $BaTiO_3$ and 0.05-0.5%wt Fe-doped $BaTiO_3$ samples. For comparison purposes, photolysis of MB was as well evaluated under the same conditions but without catalyst. It was found out that only 7.6% of MB degraded over the same irradiation time. It was observed that the doped samples exhibited better photoactivity performance. The kinetic data for methylene blue degradation under visible -light illumination were found to follow pseudo first-order as shown in figure 8 (b). The computed pseudo first order rate constants (k, min^{-1}) are illustrated in figure 8 (b).

The sample with 0.5%wt Fe load had the best performance in photodegradation of MB in aqueous solution under visible light irradiation. This better performance is due to the fact the Fe ions could act as electron traps, promoting the electron-hole separation and thus, bettering the photocatalytic activity and the interfacial charge-transfer process from catalyst to adsorbed substrate (Xu, Wang, Gao, Ren, & Wang, 2011). Furthermore, doping with transition metal ions leads to a red shift of $BaTiO_3$ absorption spectrum hence, an improved photocatalytic performance as observed. Moreover, introduction of Fe ions increases the rate of charge separation since they act as traps hence minimizing the rate of charge recombination (Guo, Li, Wang, Dong, & Wu, 2012)

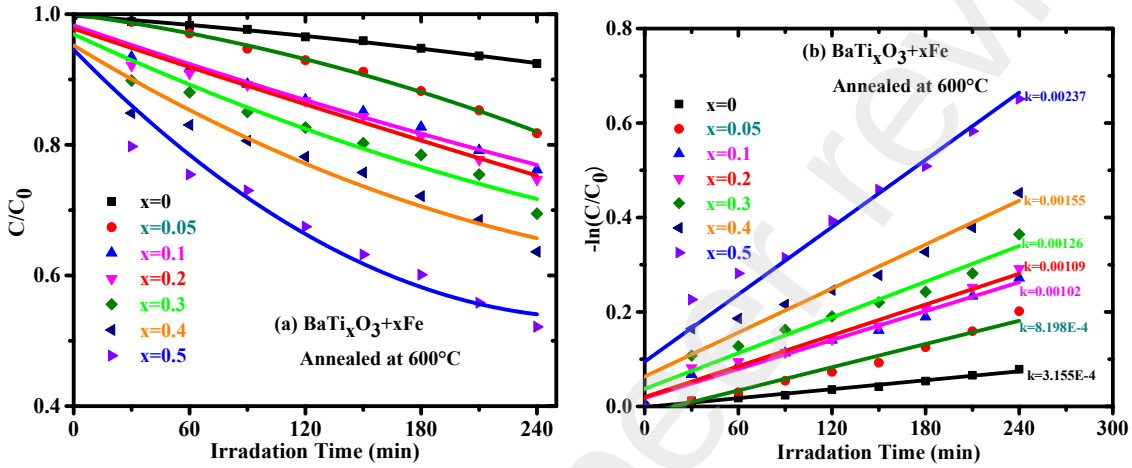

Figure. 8 (a) The degradation efficiencies of MB solution and (b) the computed pseudo first order rate constants (k, min^{-1}) over pure $BaTiO_3$ and 0.05-0.5%wt Fe-doped $BaTiO_3$ samples.

Conclusion

Undoped and Fe-doped BaTiO3 thin films on a glass substrate were synthesized through spin coating technique using titanium (iv) isopropoxide and barium acetate as the precursor solutions. The results of spectrophotometer show that 0.4%wt Fe-doped BaTiO3 had the optimum absorbance of slightly above 80% in the visible range. Doping the sample with Fe greatly reduced the bandgap from 3.26 – 1.59 eV, making the material to absorb of the radiation in the visible range region. Annealing also greatly improved material properties. The above annealing temperature was found to be 600℃. 0.5%wt Fe loaded sample had the best photocatalytic performance with degradation constant of 2.37×10^{-3} m^{-1}. Electronic studies through DFT based calculations revealed that Fe doped introduced weak coordinate covalent bonds that lead to reduction of the bandgaps of the doped samples. From the analysis, it is evident that Fe doped $BaTiO_3$ can be employed as visible light photocatalytic material.

Conflicts of Interest

The authors declare that there is no conflict of interest regarding the publication of this article.

Acknowledgement

The authors acknowledge the Kenya Education Network (KENET) CMMS mini-grant 2019 to CTheP group in MMUST, Masinde Muliro University of Science and Technology Grant No MMU/URF/2022/1-026, computing resources provided by the Centre for High Performance Computing (CHPC-MATS1426) in Cape Town, South Africa and ISP, Uppsala University for sponsorship to MSSEESA conferences.

References

Aminul, M., Addul, M., & Meherun, N. (2017). Effect of Fe doping on the structural, optical and electronic properties of BaTiO3: DFT based calculation. *Chinese Journal of Physics, Elsevier*, 731-738.

Chukwuka, A., Ilknur, A., & Vassilis, S. (2022). itanium dioxide (TiO_2)-based photocatalyst materials activity enhancement for contaminants of emerging concern. *Chemical Engineering Journal Advances*, 2666-8211. doi:https://doi.org/10.1016/j.ceja.2022.100262

Cui, Y., Briscoe, J., & Dunn, S. (2013). Effect of ferroelectricity on solar-light-driven photocatalytic activity of BaTiO3-influence on the carrier separation and stern layer formation. *Chem Mater*, 4215-4223.

Fang, R. (2023). Solid spectroscopy. *University of Science and Technology of China Press.*, 1-98.

González-Fernández, C., Gómez-Pastora, J., Bringas, E., Zborowski, M., & Chalmers, J. O. (2021). Recovery of Magnetic Catalysts: Advanced Design for Process Intensification. *Ind Eng Chem Res., 60*(46), 6780-16790. doi:10.1021/acs.iecr.1c03474. Epub 2021 Sep 22

Granqvist, C. (1995). *Handbook of Inorganic Electrochromic Materials.* Netherlands: elsevier, Amsterdam.

Guo, S., Li, X., Wang, H., Dong, F., & Wu, Z. (2012). Fe-ions modified mesoporous Bi2WO6 nanosheets with high visible light photocatalytic activity. *J. Colloid Interf. Sci*, 373-380.

Hellwege, K. (2016). Ferroelctrics and Related Substances. *New series Group 3 Springer*, 1-3.

Huaitao, Y., Beibei, Y., Wei, C., & Junjiao, Y. (2022). Preparation and Photocatalytic Activities of TiO2-Based Compoasite Catalysts. *Catalysts*, 1-39.

Kappadan, S., Gebreab, T., Thomas, S., & Kalarikkal, N. (2016). Tetragonal BaTiO3 nanoparticles: An efficient photocatalyst for the degradation of organic pollutants. *Mat Sci Semicon Proc*, 42-47.

Lee, W., Chung, W., Huang, W., Lin, W., Lin, W., Jiang, Y., & Chen, C. (2013). Photocatalytic activity and mechanism of nano-cubic barium titanate prepared by a hydrothermal method. *J Taiwan Inst Chem E*, 660-669.

Leyland, N., Podporska-Carroll, J., Browne, J., Hinder, S., Quilty, B., & Pillai, C. (2016). Highly Efficient F, Cu doped TiO2anti-bacterial visible light active photocatalytic coatings to combat hospital-acquired infections. *, Sci. Rep.*

Liu, J., & Sun, Y. (2012). Ag loaded flower-like BaTiO3 nanotube arrays: fabrication and enhanced photocatalytic property. *Crystengcomm*, 1473-1478.

Maria, C., Alessandro, A., Marco, M., Francesca, C., Vincenzo, T., Elena, R., & Sabrina, S. (2021). Disinfection of Wastewater by UV-Based Treatment for Reuse in a Circular Economy Perspective. Where Are We at? *International Journal of Environmental Research and Public Health*, 1-24. doi:https://doi.org/10.3390%2Fijerph18010077

Nurazila, Z., Mahmood, S., Thye, C., & Julie, M. (2024). X-ray Diffraction study of Crystalline Barium Titanate Ceramics. *AIP publishing*, 160-163.

Restiani, A., & Asep, N. (2022). How to Read and Interpret UV-VIS Spectrophotometric Results in Determining the Structure of Chemical Compounds. *Indonesian Journal of Educational Research and Technology*, 1-20.

Sharma, M., & Vaish, R. (2021). Piezo/pyro/photo-catalysis activities in Ba0.85Ca0.15(Ti0.9Zr0.1)1-xFexO3 ceramics. *J Am Ceram Soc.*, 45-56.

Surassa, S., Hataikarn, R., Khatcharin, W., Phanichphant, S., & Natda, W. (2014). Effect of iron loading on the photocatalytic performance of Bi2WO6 photocatalyst. *Superlattices and Microstructures*, 1-34.

Tang, H., Prasad, K., Sanjines, R., Schmid, P., & Levy, F. (1994). Electrical and Optical Properties of TiO2 Anatase Thin Films. *Journal of Applied Physics*, 2042-2047. doi:http://dx.doi.org/10.1063/1.356306

Xu, J., Wang, W., Gao, E., Ren, J., & Wang, L. (2011). Bi2WO6/Cu0: A novel coupled system with enhanced photocatalytic activity by Fenton-like synergistic effect,. *Catal. Commun*, 834-838.

Zhang, Y., Deng, H., Si, S., Wang, T., Zheng, D., & Yang, P. (2020). *J Am Ceram Soc*, 2491–24978.